AGU PUBLICATIONS

Geophysical Research Letters

RESEARCH LETTER
10.1002/2015GL067503

Key Points:
- A strengthening of the relationship between ENSO and WRST is observed in the historical record
- Summer ENSO teleconnection to the NH extratropics experienced a remarkable change
- Changes in ENSO-related tropical variability may account for the strengthened ENSO-WRST connection

Supporting Information:
- Supporting Information S1

Correspondence to:
J. Li,
ljp@bnu.edu.cn

Citation:
Sun, C., J. Li, and R. Ding (2016), Strengthening relationship between ENSO and western Russian summer surface temperature, *Geophys. Res. Lett.*, *43*, 843–851, doi:10.1002/2015GL067503.

Received 18 DEC 2015
Accepted 28 DEC 2015
Accepted article online 30 DEC 2015
Published online 21 JAN 2016

Strengthening relationship between ENSO and western Russian summer surface temperature

Cheng Sun[1,2], Jianping Li[1,2], and Ruiqiang Ding[3,4]

[1]College of Global Change and Earth System Science (GCESS), Beijing Normal University, Beijing, China, [2]Joint Center for Global Change Studies, Beijing, China, [3]State Key Laboratory of Numerical Modeling for Atmospheric Sciences and Geophysical Fluid Dynamics (LASG), Institute of Atmospheric Physics, Chinese Academy of Sciences, Beijing, China, [4]Plateau Atmosphere and Environment Key Laboratory of Sichuan Province, Chengdu University of Information Technology, Chengdu, China

Abstract Western Russia (WR) experienced an extremely hot summer in 2010 that caused tremendous social and economic losses. The WR summer surface temperature (WRST) in the observational record is characterized by substantial interannual variability superimposed on the secular warming trend. Analysis of the 130 year observational record reveals that a strong and significant inverse relationship between WRST interannual variability and the tropical El Niño–Southern Oscillation (ENSO) has emerged during the past three decades. The ENSO influence on the summer extratropical atmospheric circulation was weak before 1980 but became strong and significant afterward, showing a structure similar to the East Atlantic/WR teleconnection pattern. This pattern is associated with rising/falling upper level geopotential height over WR, which leads to the warming/cooling of surface and tropospheric air temperatures. Numerical simulations from a theoretical linear baroclinic model and Atmospheric Model Intercomparison Project models further suggest that the enhancement of the ENSO teleconnection to WR may be attributable to a change in the ENSO-related tropical thermal forcing. A tripole-type rainfall anomaly pattern over tropical Pacific and Atlantic is found to be associated with ENSO in the past three decades. The tripole heating pattern can excite a Rossby wave that extends northwestward reaching WR and is necessary for the strong influence of ENSO on WR summer climate.

1. Introduction

Significant warming trends are observed in Northern Hemisphere (NH) midlatitude land surface temperatures during the instrumental period. There is clear evidence that the warming trend is closely related to the increase in anthropogenic greenhouse gas emissions and that greater warming occurs over land than over the oceans [*Stocker et al.*, 2013]. In a warmer background climate, the number of extremely warm events over NH midlatitude land areas will increase [*Rahmstorf and Coumou*, 2011; *Diffenbaugh and Scherer,* 2011]. However, the occurrence of extreme climate events cannot be solely attributed to human-induced climate change, because the year-to-year variability of the large-scale atmospheric circulation also plays a crucial role in governing climate extremes [*Trenberth et al.*, 2015; *Wu et al.*, 2015; *Horton et al.*, 2015]. Thus, a better understanding of the mechanisms influencing the year-to-year variability at NH midlatitudes is important for a better attribution of extreme climate events to natural and human-induced causes.

The western Russia (WR) summer surface temperature (WRST) in the observational record is characterized by substantial year-to-year variability superposed on the long-term warming (Figure S1 in the supporting information). During July and August 2010, the WR region experienced an exceptionally warm summer, and extraordinarily high surface temperatures were observed over a large part of the region. This extremely warm event caused tremendous social and economic losses [*Barriopedro et al.*, 2011], and some studies have shown that the high temperatures were unprecedented, at least since instrumental records began [*Barriopedro et al.*, 2011]. Several recent studies have linked the occurrence of record-breaking high summer temperatures in WR to anthropogenically forced climate warming [*Rahmstorf and Coumou*, 2011; *Coumou and Rahmstorf*, 2012]. Alternatively, some studies have suggested that the abnormally high temperature over WR during summer 2010 was primarily due to a very persistent blocking anticyclone and was therefore a result of internal atmospheric variability [*Dole et al.*, 2011; *Matsueda*, 2011; *Schneidereit et al.*, 2012]. However, the year-to-year variability in the WRST cannot be fully explained by the monotonic warming trend [*Otto et al.*, 2012], while the internal atmospheric dynamical processes have limited implications for the predictability of such extreme climate events [*Matsueda*, 2011]. Meanwhile, the role of tropical oceanic variability in WRST has been overlooked.

El Niño–Southern Oscillation (ENSO) is one of the leading modes of global sea surface temperature (SST) year-to-year variability [*Sun et al.*, 2013] and has significant impacts on the atmospheric circulation over the NH extratropics [*Seager et al.*, 2005]. There is some evidence for a significant link between ENSO and European climate [*Brönnimann*, 2007], and the atmospheric response to ENSO over the European sector closely resembles the North Atlantic Oscillation [*Toniazzo and Scaife*, 2006; *Wu and Lin*, 2012; *Wu and Zhang*, 2015]. Most studies addressing the link between ENSO and European climate have focused on the winter season, while the impacts of ENSO on European summer climate are far less well established [*Folland et al.*, 2009]. Moreover, there has been no study linking the WRST interannual variability to ENSO, and it is not known whether ENSO can influence WR summer climate. This is not only important for the attribution of the extremely warm summer in 2010 but also has potential for the prediction of such extreme climate events.

2. Data and Methods

2.1. Data

Two sets of monthly land surface air temperature data were used in the present analysis: (1) the gridded temperature data set constructed by the Climate Research Unit (CRUTEMP4) for the period 1880–2014 [*Jones et al.*, 2012] and (2) the Goddard Institute for Space Studies homogenized surface station temperature data (GISSTEMP), also available for the period 1880–2014 [*Hansen et al.*, 1999]. The SST data sets (1880–2014) used in this study include the Hadley Centre SST data set (HadSST3) [*Kennedy et al.*, 2011] and the extended reconstruction SST version 3 (ERSST v3b) data set [*Smith and Reynolds*, 2005]. Atmospheric data (1948–2014) were obtained from the National Centers for Environmental Prediction and Atmospheric Research (NCEP-NCAR) reanalysis 1 [*Kalnay et al.*, 1996] and include fields of geopotential height and air temperature. The European Center for Medium Range Weather Forecasts 40 year Reanalysis (ERA-40) and Interim Reanalysis data (ERA-Interim) [*Uppala et al.*, 2005; *Dee et al.*, 2011] were also employed to verify the reliability of the results based on the NCEP-NCAR reanalysis product. The precipitation data (1948–2014) are from the NOAA global monthly precipitation reconstruction (PREC) data set [*Chen et al.*, 2004]. Three ENSO indices were employed in this study: Niño-3.4, Niño-4, and the multivariate ENSO index (MEI). The Niño-3.4 and Niño-4 indices are defined as area-averaged SST anomalies over 5°N–5°S, 170°–120°W and 5°N–5°S, 160°E–150°W, respectively, while the MEI is calculated from six observed variables (sea level pressure, zonal and meridional surface winds, SST, surface air temperature, and total cloudiness fraction) over the tropical Pacific [*Wolter and Timlin*, 2011]. It is available for the period 1950–2014. Summer means were constructed for SST, land surface temperature, and atmospheric data by averaging values over July and August (JA). We focus on JA because they are climatologically the warmest months of the year in WR, with mean temperatures of 21.6°C and 19.3°C, respectively. Moreover, the temporal behavior of the WRST in the 2 months is significantly correlated, and the interannual variance of WRST in JA is larger than that in June. Output from Atmospheric Model Intercomparison Project (AMIP)-style runs extending back to 1979 is also employed to examine whether the WRST-ENSO relationship in the past three decades can be reproduced by state-of-the-art models. The AMIP simulations use observed SST and sea ice to force the atmospheric component of the full global circulation models.

2.2. Linear Baroclinic Model

The Linear Baroclinic Model (LBM) used in this study consists of primitive equations for vorticity, divergence, and temperature linearized about a three-dimensional JA climatology obtained from the NCEP-NCAR reanalysis. The LBM can be solved with an externally imposed forcing and gives a steady response through adiabatic processes. The LBM used here has a horizontal resolution of T42 and 20 sigma levels in the vertical. Several dissipation and diffusion terms are included: a biharmonic horizontal diffusion with the damping time scale of one day for the shortest resolved wave, a weak vertical diffusion, Newtonian damping, and Rayleigh friction as represented by a linear drag. The latter two terms have a time scale of $(1\ \text{day})^{-1}$ at the lower boundary levels and uppermost two levels while $(10\ \text{days})^{-1}$ at other levels. Details of the model formulation are given in *Watanabe and Kimoto* [2000]. To obtain the linear atmospheric response to forcing, we integrate in time for up to 25 days. The boundary layer damping of $(1\ \text{day})^{-1}$ is sufficient to neutralize unstable baroclinic modes [*Hall and Sardeshmukh*, 1998] and ensures that the steady state response is obtained in this method. The average of the last 5 days of the integration is taken as the approximate linear response to a prescribed forcing.

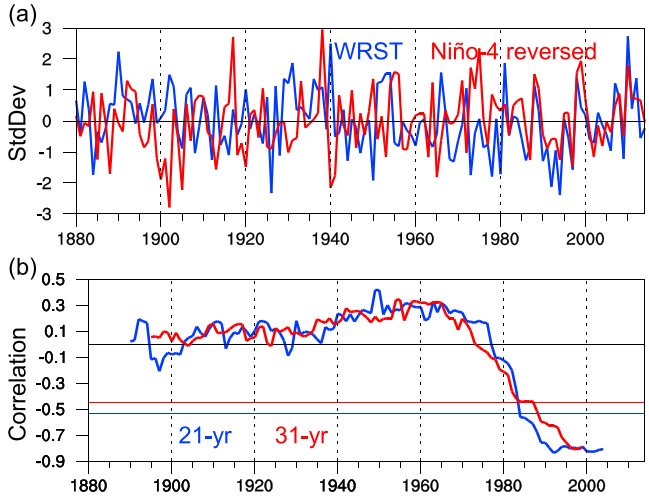

Figure 1. (a) Time series of JA WRST (blue) and Niño-4 (red) indices for 1880–2014 with the secular trends (estimated by the EEMD method) removed. For ease of comparison, the time series have been normalized by the long-term standard deviations, and the sign of the Niño-4 index has been reversed. The WRST and Niño-4 indices are derived from the CRUTEMP4 and HadSST3 data sets, respectively. (b) 21 year (blue) and 31 year (red) sliding correlations between the WRST and Niño-4 indices shown in Figure 1a. The horizontal lines show the corresponding 99% confidence level for the correlations.

3. Results

Figure 1a shows time series of the WRST and Niño-4 indices for the period 1880–2014 (with the secular trends removed) derived from the CRUTEMP4 and HadSST3 data sets, respectively. The WRST index is defined as the area-weighted average of JA surface air temperature anomalies over WR (45°–60°N, 40°–70°E). The secular trends in the WRST and Niño-4 indices are estimated using the Ensemble Empirical Mode Decomposition (EEMD) method [*Wu et al.*, 2007] and shown in the supporting information Figure S1. The WRST and Niño-4 indices both exhibit substantial interannual variability, and the relationship between them is not stationary in time. The changes in the WRST-ENSO relationship can be clearly observed in the sliding correlations on a 21 year (31 year) moving window between the WRST and Niño-4 indices (Figure 1b). The year in the *x* axis of Figure 1b indicates the central year of the 21 year (31 year) sliding window. Strong and significant negative correlations (significant at the 99% confidence level) are observed over the past few decades, while the correlations over the rest of the 1880–2014 period are relatively weak. The correlations between the WRST and ENSO are particularly high (around −0.8) since 1981, indicating that the interannual variability of WRST over the past two to three decades can be largely explained by ENSO. A similar pattern of changes in the WRST-ENSO relationship is also obtained in the analysis of the raw time series with the secular trends retained (supporting information Figure S1), suggesting that the results are independent of the secular trend. In addition, the recent strengthening of the WRST-ENSO relationship is also observed in other temperature products (e.g., GISSTEMP and ERSST), indicating that the results are robust with respect to the choice of data set (supporting information Figures S2 and S3). Moreover, the emergence of the strong WRST-ENSO correlation over recent decades is not specific to the Niño-4 index but also appears with the Niño-3.4 and MEI indices (supporting information Figures S4 and S5), suggesting that the results are not sensitive to the choice of ENSO index. Thus, the sliding correlation analysis suggests that the strong WRST-ENSO relationship in the past three decades is unprecedented over the past 130 years.

This study focuses on the strengthening relationship between WRST and ENSO. The sliding correlations (Figure 1b) show that the WRST-ENSO connection has been strongest since the beginning of the 1980s and that the relationship was very weak before 1980. Therefore, we choose the periods 1951–1980 and 1981–2010 in the following comparison analysis, with each period containing 30 years. Figures 2a and 2b show the regressions of JA land surface temperature anomalies on the Niño-4 index for the two periods 1951–1980 and 1981–2010, respectively. The spatial patterns of ENSO-related land surface temperature show notable differences between the two epochs. During 1951–1980, the land surface temperature regression shows no significant signal over middle- and high-latitude regions, while in lower latitudes (south of 30°N), the regression pattern shows warm temperature anomalies, particularly over southern Asia and southern North America. During 1981–2010, significant negative temperature anomalies associated with ENSO can be clearly observed over northern North America and WR, and the anomalies over WR are particularly strong and reach an amplitude of about 1°C. The regression results from other temperature data sets (e.g., GISSTEMP) are similar, and thus are not shown here. Therefore, these results further suggest that the WRST-ENSO connection experienced a pronounced change at the beginning of the 1980s; the ENSO influence on the WRST is weak (strong) during 1951–1980 (1981–2010).

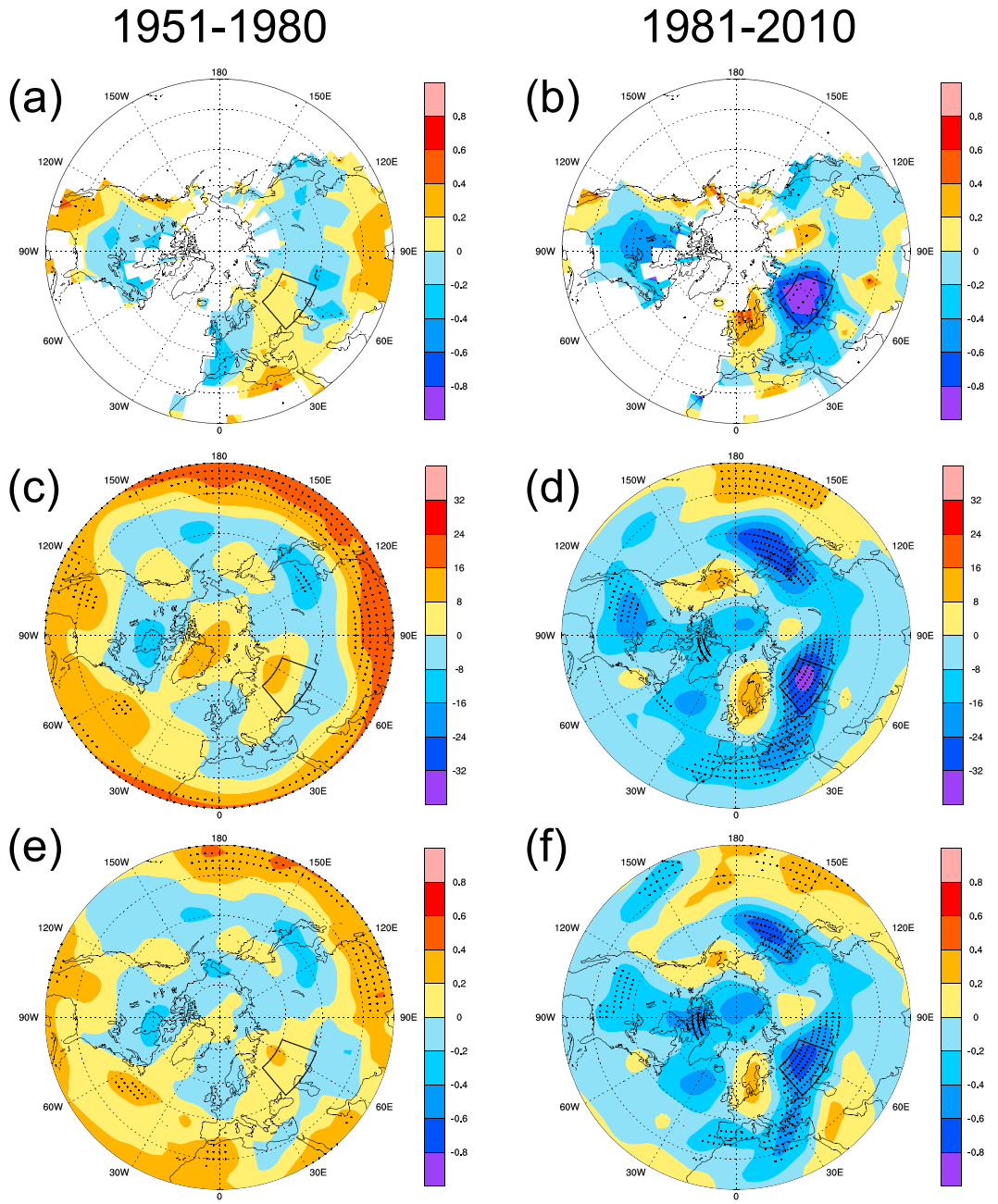

Figure 2. (a, b) Anomalies of JA land surface temperature (units: K) from CRUTEMP4, (c, d) Z200 (units: m), and (e, f) tropospheric temperature averaged between 300 and 850 hPa (units: K) from the NCAR-NCEP reanalysis data set obtained by regressions against the normalized Niño-4 index during 1951–1980 (Figures 2a, 2c, and 2e) and 1981–2010 (Figures 2b, 2d, and 2f). Dots in Figures 2a–2f indicate the regression coefficients significant at the 95% confidence level.

The changes in atmospheric circulation patterns associated with ENSO during the two epochs are also examined. Figures 2c and 2d show the regressions of JA 200-hPa geopotential height (Z200) against ENSO for 1951–1980 and 1981–2010, respectively. Pronounced changes in the ENSO-related Z200 patterns for the two epochs are evident. During 1951–1980, the Z200 pattern shows largest amplitudes over the low-latitude regions with a zonally symmetric structure, while in middle- and high-latitude regions, no significant Z200 anomalies can be found, and the amplitudes are quite small. During 1981–2010, the Z200 pattern shows multiple centers of action with significant Z200 anomalies, including a meridional dipole over the western North Pacific and an anomalous low over the WR region. The tropospheric temperature (300–850 hPa average)

patterns associated with ENSO during the two periods also exhibit remarkable changes (Figures 2e and 2f), consistent with the land surface temperature and Z200 fields. In particular, the tropospheric temperature patterns show similar spatial structures to the Z200 patterns for the two epochs, suggesting a correspondence between air temperature and atmospheric circulation fields over the extratropics. The patterns of tropospheric temperature and Z200 from the ERA-40 and ERA-Interim data (supporting information Figure S6) are similar to those from the NCEP-NCAR product, further confirming an enhanced influence on the JA NH atmospheric circulation by ENSO during the later period.

There is further correspondence between land surface air temperature and upper level atmospheric circulation. Time series of WR region averaged Z200 and tropospheric temperature anomalies for the JA season are shown in the supporting information Figure S7a. The Z200 and tropospheric temperature in this region both exhibit substantial interannual variability and are strongly positively correlated ($r = 0.88$). Moreover, the JA seasonal anomalies in Z200 are strongly correlated with the WRST ($r = 0.81$). The sliding correlations on a 31 year window between Z200 and WRST are strong and stable, with correlations around 0.8, varying by less than 0.1 (supporting information Figure S7b). These results indicate a significant coherence between upper level atmospheric circulation and land surface temperature in WR. Previous studies have suggested that the upper level atmospheric circulation over middle- and high-latitude land areas is relatively insensitive to warming or cooling of the local land surface [*Screen et al.*, 2012; *Tang et al.*, 2013]. Thus, the coherence can be understood as a response of surface and tropospheric air temperature to the adiabatic expansion/compression associated with upper level atmospheric circulation; that is, an anomalous high (low) corresponds to higher (lower) geopotential height and leads to warmer (cooler) local surface and tropospheric air temperature according to the hypsometric equation. The 31 year sliding correlations between WR region averaged Z200 and ENSO strengthen remarkably in the past three decades (supporting information Figure S7c), consistent with the sliding correlation analysis between WRST and ENSO. Therefore, the strengthening WRST-ENSO connection may be caused by the strengthened relationship between ENSO and upper level atmospheric circulation over WR.

The Z200 pattern associated with ENSO variability during 1981–2010 is marked by an anomalous low over WR flanked by weak positive height anomalies over western Europe (Figure 2d). This structure projects on the East Atlantic/WR (EA/WR) pattern, which is one of the important teleconnection patterns in the North Atlantic region [*Barnston and Livezey*, 1987]. The EA/WR pattern can be identified as the second leading empirical orthogonal function (EOF) mode of the JA atmospheric circulation variability (supporting information Figure S8), with its positive phase showing positive height anomalies over western Europe and negative anomalies over WR. The first leading EOF mode is the summer North Atlantic oscillation [*Folland et al.*, 2009]. The JA EA/WR index, given by the principal component of the EOF2 mode, shows a significant correlation with the land surface temperature ($r = -0.71$) and Z200 ($r = -0.75$) anomalies over WR (supporting information Figure S7a). The 31 year sliding correlations between EA/WR and WRST indices are significant at the 99% confidence level throughout the analysis period (supporting information Figure S7b). In addition, the sliding correlations between EA/WR and ENSO indices also indicate that a significant EA/WR-ENSO connection has emerged in the past three decades (supporting information Figure S7c). A recent study focusing on the summer Mediterranean climate has suggested that from the 1980s onward the SST dipole between tropical Atlantic and Pacific could induce an anomalous cyclonic circulation over Scandinavia surrounded by anomalous highs [*Losada et al.*, 2012]. The structure of the circulation pattern is similar to the EA/WR, further supporting the strong relationship between the EA/WR and tropical Pacific SST revealed in the present study.

Atmospheric circulation variability over extratropical regions is often related to the tropical rainfall anomaly, which provides an important heat source driving large-scale atmospheric motion [*Ding et al.*, 2011; *Wang et al.*, 2012]. Tropical rainfall and the associated diabatic heating also play a crucial role in understanding the influence of tropical SST on the extratropical atmospheric circulation [*Greatbatch et al.*, 2004; *DeWeaver and Nigam*, 2004; *Yu*, 2007]. Thus, in order to understand the enhanced WRST-ENSO relationship, we examine in more detail how the tropical rainfall (used as a proxy for tropical diabatic heating) is related to the ENSO variability. Figures 3a and 3b show the regressions of JA tropical rainfall anomalies onto the Niño-4 index for the two epochs 1951–1980 and 1981–2010, respectively. The rainfall anomalies display evident differences between the two periods. During 1951–1980, the rainfall pattern shows a monopole structure with pronounced wet anomalies over the equatorial central Pacific and the tropically averaged (20°S–20°N) rainfall basically shows anomalies of the same sign throughout the tropical region. However, during 1981–2010, the rainfall pattern is characterized by a tripole structure with wet anomalies over the equatorial central

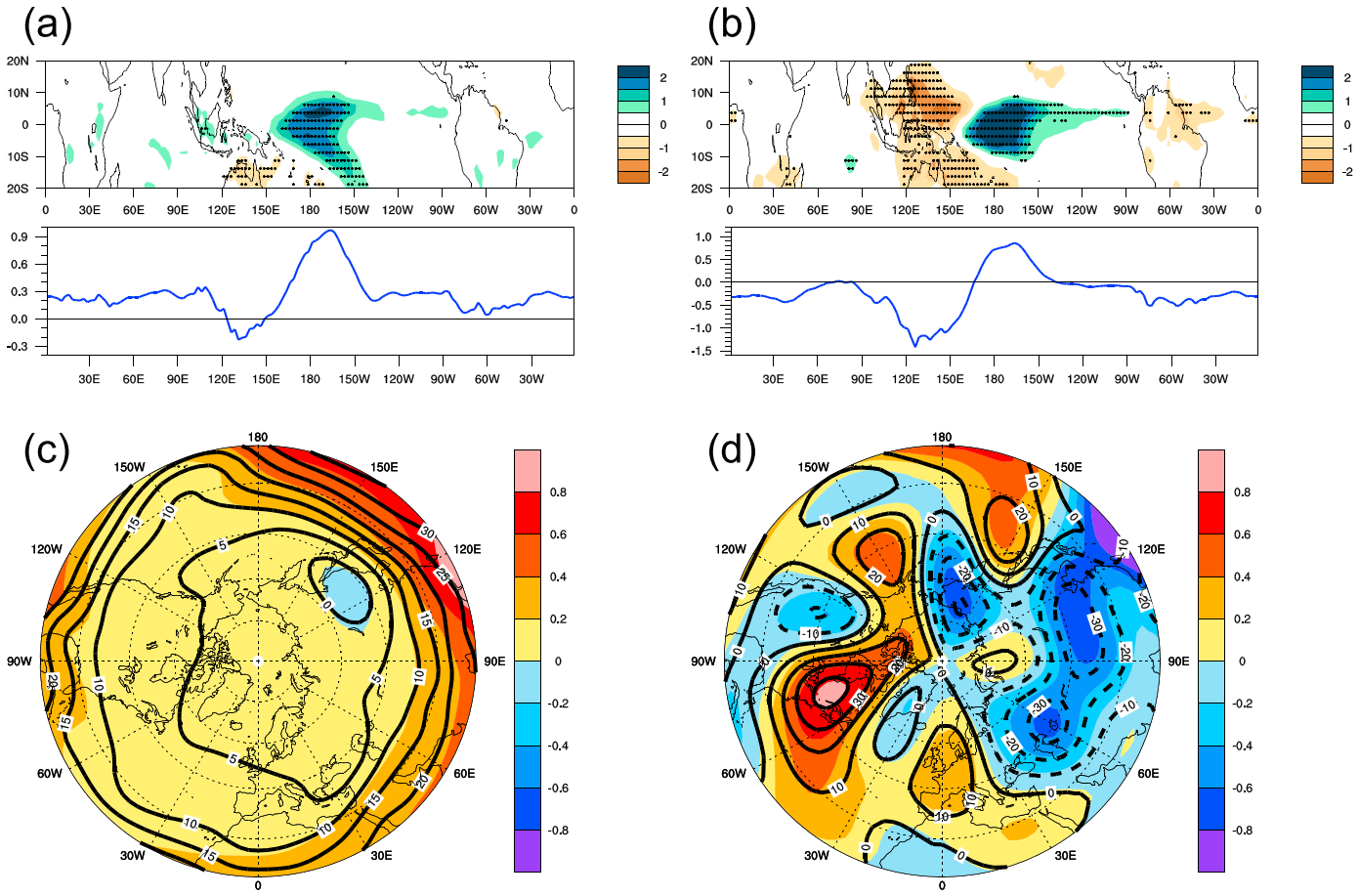

Figure 3. JA tropical rainfall anomalies (shading, units: mm d^{-1}) and the tropical averages between 20°S and 20°N (blue line) from the PREC data set regressed against the normalized Niño-4 index during (a) 1951–1980 and (b) 1981–2010. Dots in Figures 3a and 3b indicate the regression coefficients significant at the 95% confidence level. (c and d) The LBM simulations of the steady responses of tropospheric temperature averaged between 300 and 850 hPa (shading, units: K) and Z200 (contours, units: m) to the tropical thermal forcings as indicated by the rainfall anomalies in Figures 3a and 3b, respectively. Details of the construction of the tropical thermal forcings used in the LBM experiments are given in the text.

Pacific and significant dry anomalies in the tropical western Pacific and tropical Atlantic. This zonal tripole pattern is also evident for the tropically averaged rainfall anomalies. Numerous studies have suggested that an interdecadal change in the ENSO teleconnection to the tropical western Pacific occurred around 1980 [*Wang et al.*, 2008; *Xie et al.*, 2010; *Wu et al.*, 2012]. The relationship of the tropical western Pacific climate with the remote ENSO forcing has strengthened since 1980, and in particular, the tropical western Pacific has become dominated by strong and significant descending motion in response to the warm ENSO phase during the summer season. The structural change in the ENSO-related tropical SST may lead to the change in ENSO rainfall. As shown in the supporting information Figure S9, the structural change in the ENSO SST shows enhanced negative SST anomalies in tropical western Pacific and tropical Atlantic, consistent with the enhancement of dry anomalies in the ENSO rainfall over the two regions. Previous studies have also suggested a substantial anticorrelation between ENSO and tropical Atlantic SST since the late 1970s [*Kucharski et al.*, 2007; *Losada et al.*, 2012]. Moreover, the ENSO SST during recent decades exhibits increased and decreased variability over the central and eastern Pacific, respectively, which is in agreement with the increased frequency of central Pacific ENSO [*Yeh et al.*, 2009].

Increased (decreased) rainfall anomalies in the tropics correspond to more (less) condensation heat release and hence anomalous heating (cooling) in the midlevels of the tropical troposphere. Two sets of idealized thermal forcings over the tropical region, one a monopole-type forcing and the other a tripole-type forcing, are designed to mimic the diabatic heating associated with the rainfall anomalies in Figures 3a and 3b, and the LBM is employed to examine atmospheric responses to the forcings. The horizontal distributions of the

two sets of forcings are similar to the monopole and tripole patterns of rainfall anomalies shown in Figures 3a and 3b, and there is no forcing prescribed outside the tropical region. The vertical profile of the heating is displayed in the supporting information Figure S10, showing a maximum heating rate at the 0.5 sigma level, in accordance with the idealized heating profiles used in previous LBM modeling studies [*Sun et al.*, 2014]. As a result, the three-dimensional forcings can be constructed with a vertical maximum heating rate of 2 K d^{-1} around the horizontal centers. Figures 3c and 3d show the LBM-simulated atmospheric responses over the NH extratropics to the two sets of thermal forcings. For the tropical monopole heating, the response of tropospheric temperature is characterized by warm anomalies in low-latitude regions with a nearly zonally symmetric structure. The Z200 response shows a similar pattern with rising heights at low latitudes. The amplitudes of the temperature and Z200 responses over middle- and high-latitude regions are much smaller, and the responses over the WR region are also very weak. The spatial structures of the atmospheric response to the monopole heating closely resemble the atmospheric circulation patterns associated with the Niño-4 index during 1951–1980 as shown in Figure 2.

The atmosphere responds quite differently to the tropical tripole heating. The amplitudes of the responses over middle- and high-latitude regions are comparable to those in low latitudes, and in particular, the responses show strong negative Z200 anomalies and tropospheric cooling centered near the WR region. The main large-scale features of the atmospheric responses, including a meridional dipole in the western North Pacific and an EA/WR-like pattern with an anomalous low near WR, are similar to the observed pattern associated with the warm ENSO phase during 1981–2010 shown in Figure 2. The LBM-simulated responses of Z200 perturbations to the tropical tripole thermal forcing from day 5 to 20 are shown in the supporting information Figure S11. Negative height anomalies are induced to the northwest of the tropical western Pacific cooling at day 5, corresponding to the Rossby wave response associated with the Gill-type circulation [*Gill*, 1980]. After day 5, the negative anomalies spread northwestward toward the region northeast of the Mediterranean Sea. At day 20, the negative anomalies cover most of WR, and the pattern of the response becomes stable. There is substantial evidence from modeling that the diabatic heating associated with tropical Asian monsoon rains is linked to the summer climate in the Mediterranean and surrounding regions through heating-induced Rossby waves that extend northwestward [*Rodwell and Hoskins*, 2001; *Lin*, 2009]. Thus, the mechanism for the simulated response over WR to the tropical tripole heating is consistent with the previous modeling studies. Moreover, the LBM simulation results suggest that the observed enhancement in the ENSO teleconnection to WR is due primarily to the changes in the ENSO-related tropical forcing.

As shown in the supporting information Figure S12, four models from the AMIP simulations can reproduce the significant negative correlation between JA WRST and ENSO in the past three decades, but only two of these four models capture the observed teleconnection between ENSO and WR-averaged Z200, which is necessary for understanding the WRST-ENSO connection. The two models are Fgloals-g2 and MRI-CGCM3. The simulated JA surface temperature and Z200 in response to the warm ENSO phase from these two models are shown in the supporting information Figure S13. The patterns of surface temperature and Z200 are generally similar in the two models. The simulated surface temperature shows significant cool anomalies in the WR region, consistent with the observed temperature pattern associated with ENSO during 1981–2010. The simulated Z200 field also bears a strong resemblance to the observations, with a meridional dipole structure over the North Pacific and an EA/WR-like teleconnection pattern. The simulated JA tropical rainfall anomalies in response to a warm ENSO phase are shown in the supporting information Figure S14. There is strong agreement with the observed rainfall pattern during 1981–2010 in Figure 3b. The simulated tropical rainfall patterns from the two models are similar, both marked by a zonal tripole structure with wet anomalies in the central tropical Pacific and dry anomalies in the western tropical Pacific and tropical Atlantic, corresponding to the tripole-type thermal forcing. Therefore, the AMIP simulations provide further modeling evidence that the tripole-type tropical forcing is necessary for the significant ENSO teleconnection to WR during the past three decades.

4. Conclusion and Discussion

The western Russian summer (July and August) surface temperature (WRST) exhibits substantial interannual variability in addition to the monotonic long-term warming trend. This interannual variability is important for understanding the occurrence of extreme climate events, such as the record-breaking hot summer of 2010.

The present study provides observational evidence that the interannual WRST has been closely linked to the tropical ENSO during the past three decades with the WRST showing significant cool (warm) anomalies in association with a warm (cool) ENSO phase. This strong WRST-ENSO connection is unprecedented in the observational records. The strengthening of the WRST-ENSO relationship is related to the change in the extratropical atmospheric circulation response to ENSO. During 1951–1980, the influence of ENSO on summer middle- and high-latitude circulation variability was weak and insignificant. In contrast, during 1981–2010, the upper level geopotential height showed an EA/WR-like pattern over the North Atlantic sector with a strong anomalous low (high) over WR in response to a warm (cool) ENSO phase; these lower (higher) geopotential heights can then lead to surface and tropospheric cooling (warming) through adiabatic processes. Numerical simulations from simplified LBM and AMIP models further suggest that the enhancement of the ENSO teleconnection to WR may be attributable to the change in the ENSO-related tropical forcing as represented by the tropical rainfall field. A tripole-type tropical forcing pattern associated with ENSO during the past three decades is necessary for the significant influence of ENSO on the WR summer climate.

There are still some interesting questions to be answered. Several modeling studies have suggested that the changes in the ENSO teleconnections during boreal winter are related to anthropogenic global warming and that the increased greenhouse gas level may lead to changes in the strength and position of the ENSO teleconnection patterns [*Meehl and Teng,* 2007]. A number of other studies have suggested that internal decadal climate variability also influences the ENSO teleconnections. For example, recent studies have shown that the interdecadal Pacific oscillation (IPO) [*Parker et al.*, 2007] strongly modulates the interannual influence of ENSO on the Southern Hemisphere (SH) climate [*Power et al.*, 2006]. The ENSO teleconnection to the SH tends to be relatively strong during the negative IPO phase, while it becomes weaker for the positive IPO phase. Other studies have shown that the Atlantic multidecadal oscillation (AMO) [*Li et al.*, 2013] can lead to a multidecadal modulation of ENSO activity [*Kang et al.*, 2014] and hence to ENSO teleconnections to remote regions [*Kang et al.*, 2015]. The present study identifies the changes in the summer ENSO teleconnections to the NH extratropical regions around the early 1980s. Thus, further studies are required to address the question of whether these changes are attributable to anthropogenic global warming or whether they are related to internal decadal climate variability (e.g., IPO and AMO). In addition, the summer ENSO teleconnections have been investigated using AMIP-type simulations in the present analysis, and further studies using fully coupled models are needed.

Acknowledgments

The AMIP output data used in this study are available from the Coupled Model Intercomparison Project Phase 5. We acknowledge the World Climate Research Programme's Working Group on Coupled Modelling and the climate modeling groups for producing and making available their model output. We would like to thank Masahiro Watanabe at University of Tokyo for kindly providing us with the Linear Baroclinic Model. This work was jointly supported by the NSFC project 41405128 and the National Programme on Global Change and Air-Sea Interaction (GASI-IPOVAI-06).

References

Barnston, A. G., and R. E. Livezey (1987), Classification, seasonality and persistence of low-frequency atmospheric circulation patterns, *Mon. Weather Rev.*, *115*(6), 1083–1126.

Barriopedro, D., E. M. Fischer, J. Luterbacher, R. Trigo, and R. Garcia-Herrera (2011), The hot summer of 2010: Redrawing the temperature record map of Europe, *Science*, *332*(6026), 220–224.

Brönnimann, S. (2007), Impact of El Niño-Southern Oscillation on European climate, *Rev. Geophys.*, *45*, RG3003, doi:10.1029/2006RG000199.

Chen, M., P. Xie, J. E. Janowiak, and P. A. Arkin (2004), Verifying the reanalysis and climate models outputs using a 56-year data set of reconstructed global precipitation, paper presented at 14th AMS Conference on Applied Meteorology, Am. Meteorol. Soc., Seattle, Wash., 11–15 Jan.

Coumou, D., and S. Rahmstorf (2012), A decade of weather extremes, *Nat. Clim. Change*, *2*(7), 491–496.

Dee, D. P., et al. (2011), The ERA-Interim reanalysis: Configuration and performance of the data assimilation system, *Q. J. R. Meteorol. Soc.*, *137*(656), 553–597.

DeWeaver, E., and S. Nigam (2004), On the forcing of ENSO teleconnections by anomalous heating and cooling, *J. Clim.*, *17*(16), 3225–3235.

Diffenbaugh, N. S., and M. Scherer (2011), Observational and model evidence of global emergence of permanent, unprecedented heat in the 20th and 21st centuries, *Clim. Change*, *107*, 615–624.

Ding, Q. H., B. Wang, J. M. Wallace, and G. Branstator (2011), Tropical-extratropical teleconnections in boreal summer: Observed interannual variability, *J. Clim.*, *24*(7), 1878–1896.

Dole, R., M. Hoerling, J. Perlwitz, J. Eischeid, P. Pegion, T. Zhang, X.-W. Quan, T. Xu, and D. Murray (2011), Was there a basis for anticipating the 2010 Russian heat wave?, *Geophys. Res. Lett.*, *38*, L06702, doi:10.1029/2010GL046582.

Folland, C. K., J. Knight, H. W. Linderholm, D. Fereday, S. Ineson, and J. W. Hurrell (2009), The summer North Atlantic oscillation: Past, present, and future, *J. Clim.*, *22*(5), 1082–1103.

Gill, A. E. (1980), Some simple solutions for heat-induced tropical circulation, *Q. J. R. Meteorol. Soc.*, *106*(449), 447–462.

Greatbatch, R. J., J. Lu, and K. A. Peterson (2004), Nonstationary impact of ENSO on Euro-Atlantic winter climate, *Geophys. Res. Lett.*, *31*, L02208, doi:10.1029/2003GL018542.

Hall, N. M. J., and P. D. Sardeshmukh (1998), Is the time-mean Northern Hemisphere flow baroclinically unstable?, *J. Atmos. Sci.*, *55*(1), 41–56.

Hansen, J., R. Ruedy, J. Glascoe, and M. Sato (1999), GISS analysis of surface temperature change, *J. Geophys. Res.*, *104*(D24), 30,997–31,022, doi:10.1029/1999JD900835.

Horton, D. E., N. C. Johnson, D. Singh, D. L. Swain, B. Rajaratnam, and N. S. Diffenbaugh (2015), Contribution of changes in atmospheric circulation patterns to extreme temperature trends, *Nature*, *522*(7557), 465–469.

Jones, P. D., D. H. Lister, T. J. Osborn, C. Harpham, M. Salmon, and C. P. Morice (2012), Hemispheric and large-scale land-surface air temperature variations: An extensive revision and an update to 2010, *J. Geophys. Res.*, *117*, D05127, doi:10.1029/2011JD017139.
Kalnay, E., et al. (1996), The NCEP/NCAR 40-year reanalysis project, *Bull. Am. Meteorol. Soc.*, *77*(3), 437–471.
Kang, I. S., H. H. No, and F. Kucharski (2014), ENSO amplitude modulation associated with the mean SST changes in the tropical central Pacific induced by Atlantic multidecadal oscillation, *J. Clim.*, *27*(20), 7911–7920.
Kang, I. S., I. U. Rashid, F. Kucharski, M. Almazroui, and A. K. Alkhalaf (2015), Multidecadal changes in the relationship between ENSO and wet-season precipitation in the Arabian peninsula, *J. Clim.*, *28*(12), 4743–4752.
Kennedy, J. J., N. A. Rayner, R. O. Smith, D. E. Parker, and M. Saunby (2011), Reassessing biases and other uncertainties in sea surface temperature observations measured in situ since 1850: 1. Measurement and sampling uncertainties, *J. Geophys. Res.*, *116*, D14103, doi:10.1029/2010JD015218.
Kucharski, F., A. Bracco, J. H. Yoo, and F. Molteni (2007), Low-frequency variability of the Indian monsoon-ENSO relationship and the tropical Atlantic: The "weakening" of the 1980s and 1990s, *J. Clim.*, *20*(16), 4255–4266.
Li, J. P., C. Sun, and F. F. Jin (2013), NAO implicated as a predictor of Northern Hemisphere mean temperature multidecadal variability, *Geophys. Res. Lett.*, *40*, 5497–5502, doi:10.1002/2013GL057877.
Lin, H. (2009), Global extratropical response to diabatic heating variability of the Asian summer monsoon, *J. Atmos. Sci.*, *66*(9), 2697–2713.
Losada, T., B. Rodriguez-Fonseca, and F. Kucharski (2012), Tropical influence on the summer Mediterranean climate, *Atmos. Sci. Lett.*, *13*(1), 36–42.
Matsueda, M. (2011), Predictability of Euro-Russian blocking in summer of 2010, *Geophys. Res. Lett.*, *38*, L06801, doi:10.1029/2010GL046557.
Meehl, G. A., and H. Y. Teng (2007), Multi-model changes in El Niño teleconnections over North America in a future warmer climate, *Clim. Dyn.*, *29*(7–8), 779–790.
Otto, F. E. L., N. Massey, G. J. van Oldenborgh, R. G. Jones, and M. R. Allen (2012), Reconciling two approaches to attribution of the 2010 Russian heat wave, *Geophys. Res. Lett.*, *39*, L04702, doi:10.1029/2011GL050422.
Parker, D., C. Folland, A. Scaife, J. Knight, A. Colman, P. Baines, and B. W. Dong (2007), Decadal to multidecadal variability and the climate change background, *J. Geophys. Res.*, *112*, D18115, doi:10.1029/2007JD008411.
Power, S., M. Haylock, R. Colman, and X. D. Wang (2006), The predictability of interdecadal changes in ENSO activity and ENSO teleconnections, *J. Clim.*, *19*(19), 4755–4771.
Rahmstorf, S., and D. Coumou (2011), Increase of extreme events in a warming world, *Proc. Natl. Acad. Sci. U.S.A.*, *108*(44), 17,905–17,909.
Rodwell, M. J., and B. J. Hoskins (2001), Subtropical anticyclones and summer monsoons, *J. Clim.*, *14*(15), 3192–3211.
Schneidereit, A., S. Schubert, P. Vargin, F. Lunkeit, X. H. Zhu, D. H. W. Peters, and K. Fraedrich (2012), Large-scale flow and the long-lasting blocking high over Russia: Summer 2010, *Mon. Weather Rev.*, *140*(9), 2967–2981.
Screen, J. A., C. Deser, and I. Simmonds (2012), Local and remote controls on observed arctic warming, *Geophys. Res. Lett.*, *39*, L10709, doi:10.1029/2012GL051598.
Seager, R., N. Harnik, W. A. Robinson, Y. Kushnir, M. Ting, H. P. Huang, and J. Velez (2005), Mechanisms of ENSO-forcing of hemispherically symmetric precipitation variability, *Q. J. R. Meteorol. Soc.*, *131*(608), 1501–1527.
Smith, T. M., and R. W. Reynolds (2005), A global merged land-air-sea surface temperature reconstruction based on historical observations (1880–1997), *J. Clim.*, *18*(12), 2021–2036.
Stocker, T. F., et al. (2013), Climate change 2013: The physical science basis—Summary for policymakers, in *Climate Change 2013: The Physical Science Basis. Contribution of Working Group 1 to the Fifth Assessment Report of the Intergovernmental Panel on Climate Change*, edited by T. F. Stocker et al., pp. 2–29, Cambridge Univ. Press, Cambridge, U. K., and New York.
Sun, C., J. P. Li, F. F. Jin, and R. Q. Ding (2013), Sea surface temperature inter-hemispheric dipole and its relation to tropical precipitation, *Environ. Res. Lett.*, *8*(4), doi:10.1088/1748-9326/8/4/044006.
Sun, C., J. P. Li, F. F. Jin, and F. Xie (2014), Contrasting meridional structures of stratospheric and tropospheric planetary wave variability in the Northern Hemisphere, *Tellus A*, *66*, doi:10.3402/tellusa.v66.25303.
Tang, Q. H., X. J. Zhang, X. H. Yang, and J. A. Francis (2013), Cold winter extremes in northern continents linked to arctic sea ice loss, *Environ. Res. Lett.*, *8*(1), 014036, doi:10.1088/1748-9326/8/1/014036.
Toniazzo, T., and A. A. Scaife (2006), The influence of ENSO on winter North Atlantic climate, *Geophys. Res. Lett.*, *33*, L24704, doi:10.1029/2006GL027881.
Trenberth, K. E., J. T. Fasullo, and T. G. Shepherd (2015), Attribution of climate extreme events, *Nat. Clim. Change*, *5*(8), 725–730.
Uppala, S. M., et al. (2005), The ERA-40 re-analysis, *Q. J. R. Meteorol. Soc.*, *131*, 2961–3012.
Wang, B., J. Yang, and T. Zhou (2008), Interdecadal changes in the major modes of Asian–Australian monsoon variability: Strengthening relationship with ENSO since the late 1970s*, *J. Clim.*, *21*(8), 1771–1789.
Wang, H., B. Wang, F. Huang, Q. Ding, and J.-Y. Lee (2012), Interdecadal change of the boreal summer circumglobal teleconnection (1958–2010), *Geophys. Res. Lett.*, *39*, L12704, doi:10.1029/2012GL052371.
Watanabe, M., and M. Kimoto (2000), Atmosphere–ocean thermal coupling in the North Atlantic: A positive feedback, *Q. J. R. Meteorol. Soc.*, *126*(570), 3343–3369.
Wolter, K., and M. S. Timlin (2011), El Niño/Southern Oscillation behaviour since 1871 as diagnosed in an extended multivariate ENSO index (mei.Ext), *Int. J. Climatol.*, *31*(7), 1074–1087.
Wu, Z. H., N. E. Huang, S. R. Long, and C. K. Peng (2007), On the trend, detrending, and variability of nonlinear and nonstationary time series, *Proc. Natl. Acad. Sci. U.S.A.*, *104*(38), 14,889–14,894.
Wu, Z. W., and H. Lin (2012), Interdecadal variability of the ENSO-North Atlantic oscillation connection in boreal summer, *Q. J. R. Meteorol. Soc.*, *138*(667), 1668–1675.
Wu, Z. W., and P. Zhang (2015), Interdecadal variability of the mega-ENSO-NAO synchronization in winter, *Clim. Dyn.*, *45*(3–4), 1117–1128.
Wu, Z. W., J. Li, Z. Jiang, and T. Ma (2012), Modulation of the Tibetan Plateau snow cover on the ENSO teleconnections: From the East Asian summer monsoon perspective, *J. Clim.*, *25*, 2481–2489.
Wu, Z. W., P. Zhang, H. Chen, and Y. Li (2015), Can the Tibetan plateau snow cover influence the interannual variations of Eurasian heat wave frequency?, *Clim. Dyn.*, *45*, doi:10.1007/s00382-015-2775-y.
Xie, S. P., Y. Du, G. Huang, X. T. Zheng, H. Tokinaga, K. M. Hu, and Q. Y. Liu (2010), Decadal shift in El Niño influences on indo-western pacific and east Asian climate in the 1970s, *J. Clim.*, *23*(12), 3352–3368.
Yeh, S.-W., J.-S. Kug, B. Dewitte, M.-H. Kwon, B. Kirtman, and F.-F. Jin (2009), El Niño in a changing climate, *Nature*, *461*, 511–514.
Yu, B. (2007), The Pacific-North American pattern associated diabatic heating and its relationship to ENSO, *Atmos. Sci. Lett.*, *8*(4), 107–112.